Numerical investigation of the logarithmic Schrödinger model of quantum decoherence

Rory van Geleuken and Andrew V. Martin*
School of Science, RMIT University, Melbourne, Victoria 3000, Australia

(Received 24 June 2021; accepted 28 February 2022; published 25 March 2022)

A logarithmic Schrödinger equation with time-dependent coupling to the nonlinearity is presented as a model of collisional decoherence of the wave function of a quantum particle in position space. The particular mathematical form of the logarithmic Schrödinger equation has been shown to follow from conditional wave theory, but the validity of the logarithmic Schrödinger equation has not yet been investigated numerically for general initial conditions. Using an operator-splitting approach, we solve the nonlinear equation of motion for the wave function numerically and compare it to the solution of the standard Joos-Zeh master equation for the density matrix. We find good agreement for the time-dependent behavior of the ensemble widths between the two approaches, but note curious zero-pinning behavior of the logarithmic Schrödinger equation, whereby the zeros of the wave function are not erased by continued propagation. By examining the derivation of the logarithmic Schrödinger equation from conditional wave theory, we indicate possible avenues of resolution to this zero-pinning problem.

DOI: 10.1103/PhysRevA.105.032210

I. INTRODUCTION

Understanding the behavior of a quantum system under the continuous influence of its environment is of prime importance to a wide variety of research areas, ranging from fundamental questions about the quantum-to-classical transition [1–3] to the creation and operation of emerging quantum technologies [4]. In the case of the latter, modeling the effects of decoherence by the environment is a significant step in the design and implementation of these new technologies, where the loss of coherence between states is often a limiting factor [5]. However, the macroscopic number of degrees of freedom of any physically reasonable environmental model results in analytically intractable models for the interactions and so these must be treated approximately. Typically, a master equation is used, where the effects of a large class of environmental models, such as those obeying the Born and Markov approximations, can be incorporated on general principles by the addition of terms of Lindblad form [6].

If we consider a quantum particle interacting with an environment of scattering particles, the Gallis-Fleming master equation [7] can be used to describe the environment's decohering effects in position space. It is the loss of coherence between position-space basis states that is responsible for the localization of quantum particles, a feature that is completely absent in the bare Schrödinger equation. The Gallis-Fleming master equation provides a very general description of this process and was rederived and corrected by Hornberger and Sipe [8], after first being considered in approximate form by Joos and Zeh [3]. This has been used to model the effects of environmental engineering in matter-wave interferometry [9], to study the quantum-to-classical transition [1,10], and in modeling the behavior of quantum states of matter, such as Bose-Einstein condensates [11].

Treating the environment as a bath of harmonic oscillators leads to the quantum Brownian motion model, originally derived by Caldeira and Leggett [12] using path-integral techniques introduced by Feynman and Vernon [13] and solved analytically by Fleming *et al.* [14]. This model, specialized appropriately to the physical situation, has been used to study a variety of emerging quantum technologies, such as the decoherence of Josephson junctions [15], QED cavities [16], and photonic devices [17], among others [18].

A significant practical consideration in the implementation of these models is the computational complexity entailed by working with density matrices. The resources required to propagate such equations scale at least with the square of the size of the state space under consideration.

In contrast to working with density matrices, the phase-space formalism, initially developed by Groenewald [19] and independently by Moyal [20], building on ideas from Wigner [21] and others [22], involves converting the master-equation formalism into a description of the evolution of a quasiprobability distribution on phase space. This has been used very successfully to describe a wide variety of applications, such as the effects of decoherence in matter-wave interferometry [23], modeling the behavior of quantum walks as a basis for novel quantum algorithms [24], modeling fundamental tests of quantum mechanics in cavity QED [25], and even furnishing descriptions of coherent dynamics in the early universe [26]. The flexibility of phase-space approaches is hindered, as in the case of the density-matrix formalism, by the growth of the computational complexity of numerical propagation in higher-dimensional settings. This is because the Wigner-Weyl transformation between the density-matrix description and the Wigner function description is invertible and so both necessarily contain the same number of degrees of freedom.

*Corresponding author: andrew.martin@rmit.edu.au

The use of stochastic methods as a way of circumventing this computational scaling of master equations was pioneered by the quantum state diffusion methods of Gisin and Percival [27]. They showed that the solution to a large class of master equations could be modeled by the evolution of a stochastic Schrödinger equation with appropriately chosen stochastic forcing terms. Such calculations would result in a wave function that evolved in a nondeterministic manner, in response to the constant and random influence of the system's environment. The total history of a wave function calculated in such a way is known as a stochastic unraveling. In essence, these amount to samples in a Monte Carlo numerical integration scheme of the path-integral formulation, with each path corresponding to an unraveling, and can offer significant computational advantages over master-equation methods [28]. Additionally, conceptual insight into the interpretation of quantum mechanics with open systems offered by stochastic methods has been leveraged in proposals of modified theories of quantum mechanics such as the spontaneous collapse model of Ghirardi, Rimini, and Weber [29] and the subsequent continuous spontaneous localization model of Ghirardi, Pearle, and Rimini [30]. Extensions to relate these models to gravitation have also been proposed by Diósi [31] and Penrose [32].

Even with these conceptual and numerical advantages in many applications, stochastic methods cannot guarantee an increase in performance in general. This is because for complex systems, the benefit of only having to propagate wave functions rather than density matrices is outweighed by the cost of requiring large sample sizes to ensure weak convergence (which is to say, convergence at the ensemble level, rather than convergence at the level of a single unraveling, or so-called strong convergence) [33]. Although various powerful schemes for reducing necessary sample sizes exist in specific applications of stochastic evolutions [34,35], there is no known general method for reducing the inherent statistical error below that guaranteed by the central limit theorem. For many applications of stochastic quantum propagation, this is not a problem, as the value in such methods often lies in (but is not limited to) the reproduction of realistic evolutions of a system of interest, for example. However, for the description of effects such as decoherence, a well-converged density matrix or equivalent is necessary, and in this respect, stochastic methods may not be able to outperform the master-equation formalism in general.

Recently we proposed an alternative approach to performing decoherence calculations at the wave-function level called conditional wave theory (CWT) [36]. This approach uses a factorization of the many-body wave function into conditional and marginal wave functions, which was first introduced by Hunter [37] and later formed the basis for the exact factorization approach to molecular physics [38]. In molecular physics, it has been extensively developed to model, for example, light-matter interactions [39], nonadiabatic dynamics [40], and electronic decoherence [41]. It also been used to model electron microscope images [42].

In the CWT decoherence model, the marginal wave function informs about the probability density of a particle in a position space, while the conditional wave function encodes the state of the environment. We have shown in Ref. [36] that the formalism is deterministic and involves a infinite number of coupled nonlinear equations. However, this series can be truncated at three for Gaussian packets and produces results in exact agreement with a known analytic solution to a classic decoherence model. For non-Gaussian states, such a low-order truncation of the CWT equations would be an approximation. Yet if this approximation were accurate enough, it could provide a deterministic wave-function-level approach to decoherence calculations, at the expense of working with a nonlinear equation. The aim of the present study is to investigate the accuracy of this approach.

With truncated CWT equations, the marginal equation of motion takes the form of a logarithmic Schrödinger equation (LSE). This is a surprising connection to the original proposal for the LSE as a nonlinear extension of quantum mechanics due to the separability property and existence of solitonic 'Gausson' solutions [43,44]. In that work, the bounded solutions of the LSE were seen as a plausible model of macroscopic objects. However, this idea was not supported by the results of atomic physics experiments [45]. It is somewhat unexpected that the LSE reemerged as the result of a rigorous derivation in the context of CWT. In the CWT decoherence model, the sign of the nonlinearity is opposite to that of the theory of Bialynicki-Birula and Mycielsky and only unbounded solutions are possible. As a deterministic wave-function level description, CWT offers an intriguing alternative to density matrices, phase-space methods, and stochastic methods.

The LSE itself has been adapted to a variety of different fields, such as nuclear physics [46] and in modeling solitonic behavior of optically nonlinear media [47]. It has also been proposed as a model of quantum information exchange [48] and Bose-Einstein condensation [49], due to its obvious formal similarity to the expression for entropy. In contrast to these proposals, the logarithmic nonlinearity arises from the CWT description of collisional decoherence, rather than as a speculative model.

We are motivated to develop the LSE approach to decoherence further, because there may be complex decoherence calculations where CWT offers advantages over current methods. Phase-space methods have provided analytic models for matter-wave interferometry, exploiting the slit-based optical elements and one effective transverse dimension [23]. It is not inconceivable that, in the future, matter-wave experiments could involve more complex optical elements that are less amenable to the phase-space approach. Alternatively, ultracold gases are routinely formed in three dimensions and subject to complex dynamics, which could be a potential application for CWT. Before we can explore these possibilities, we need to ensure that the CWT approach, using an approximate LSE model, can correctly model the physics of decoherence for a general wave function. To investigate this, we must first test the LSE model of decoherence on non-Gaussian states in a single dimension. Note that we are not aiming to show that CWT can outperform existing methods computationally on these simple systems.

Rather, our aim in this paper is to gain physical insight into the dynamics modeled by the LSE in the context of decoherence and the validity of the approximations that lead to the LSE. To that end, in this work we investigate the LSE model

of decoherence for both Gaussian and non-Gaussian wave packets using numerical techniques. In Secs. II A and II B we briefly review the Joos-Zeh master equation and conditional wave theory, as well as the mathematical form of the corresponding LSE predicted by the latter. In Sec. II C the regularization of the logarithmic nonlinearity is discussed and in Sec. II D important properties of error propagation in partial differential equations (PDEs) with time-dependent nonlinear terms, such as the LSE given by CWT, are discussed. Section III contains the results of our numerical investigation, with Gaussian (Sec. III A) and non-Gaussian (Sec. III C) initial conditions presented. Section III D contains an analysis of the behavior of the numerical error and the nature of the agreement between the Joos-Zeh master equation (JZME) and LSE. Section IV contains a discussion of the advantages and disadvantages of the methods presented, as well as in-depth analysis of the curious zero-pinning behavior exhibited by the LSE in Sec. IV.

II. THEORY

A. Joos-Zeh master equation and conditional wave theory

A seminal result in the theory of quantum decoherence and localization was the JZME. Joos and Zeh considered a massive particle with position x that scatters massless (or approximately massless) environmental particles and found that the net effect of a macroscopic number of these events could be approximated by a simple quadratic decohering term. The regime in which the JZME's approximations hold is that of low-momentum environmental particles and small displacements of the central particle. With these conditions satisfied, the JZME governs the behavior of the reduced density matrix $\rho_S(x,x')$ of a particle moving along the x axis,

$$\frac{d}{dt}\rho_S(x,x',t) = \frac{i\hbar}{2m}\left(\frac{\partial^2}{\partial x^2} - \frac{\partial^2}{\partial x'^2}\right)\rho_S(x,x',t) - \frac{\Lambda}{\hbar}(x-x')^2\rho_S(x,x',t), \tag{1}$$

where Λ is the decoherence parameter, which controls the strength of the decohering effect of the environment. The reduced density matrix $\rho_S(x,x')$ is related to the total system-environment density matrix $\hat{\rho}$ through the partial trace,

$$\rho_S(x,x') = \langle x'|\mathrm{tr}_E\hat{\rho}|x\rangle = \sum_{|e\rangle\in\mathcal{B}_E}\langle x'|\otimes\langle e|\hat{\rho}|e\rangle\otimes|x\rangle, \tag{2}$$

where $\mathcal{B}_E$ is an orthonormal basis of $\mathcal{H}_E$, the Hilbert space of environmental states, and $\otimes$ denotes the tensor product. Using the tools of conditional wave theory, we have shown in a prior work [36] that, instead of the master-equation formalism, decoherence can be modeled by a pair of coupled equations of motion for the conditional wave function ϕ and marginal wave function a. These are defined by a factorization of the total system-plus-environment wave function ψ, through

$$\psi(x,q,t) = \phi(x,q,t)a(x,t), \tag{3}$$

where x is the coordinate of the central particle of interest (the system) and q is an abstract coordinate that represents the configuration of the environment. The factorization is not unique and has an associated gauge symmetry realized by multiplying one factor by an x-dependent phase factor and the other factor by the conjugate of the same. Nonetheless, by choosing an appropriate gauge and constructing the marginal density matrix, given by $\rho_m(x,x',t) = a^*(x',t)a(x,t)$, the resulting equation of motion can be compared to the JZME. We find a logarithmic Schrödinger equation of the form

$$i\frac{da(x,t)}{dt} = -\frac{\hbar}{2m}\nabla^2 a(x,t) + \frac{\hbar\gamma(t)}{m}a(x,t)\ln|a(x,t)|^2, \tag{4}$$

where $\gamma(t)$ is a real-valued function of time that reproduces the behavior of solutions to the JZME in coordinate space, provided the environmental state is Gaussian in its coordinate. The details of the derivation can be found in the Appendix.

The time dependence of the coupling parameter $\gamma(t)$ can be derived exactly for Gaussian initial conditions and approximately generalized to non-Gaussian initial conditions, where it possesses asymptotically linear forms in both the long- and short-time regimes. As our aim is to solve Eq. (4) for non-Gaussian initial conditions, the asymptotic behavior exhibited by $\gamma(t)$ results in a straightforward and computationally efficient numerical implementation. However, due to the nature of error propagation in nonlinear PDEs, this linearly increasing coupling leads to numerical breakdown in finite time, as discussed in Sec. II D.

B. Time dependence of the coupling to the nonlinearity

As shown in the paper by Joos and Zeh [3] where it first appeared, the JZME not only preserves the Gaussian functional form of states (so that initially Gaussian states remain Gaussian for all time) but also causes $O(t^3)$ spreading of the ensemble width $w(t)$ of these states (which corresponds to the standard deviation of the associated probability distributions). For a free particle, the Schrödinger equation predicts a linear growth rate for $w(t)$. Note that $w(t)$ is often referred to as the ensemble width, as it represents the standard deviation of a probability distribution and to distinguish it from the coherence length, which represents the distance over which a given state retains quantum phase information and hence can support superpositions.

These two length scales can be more directly interpreted in terms of the density matrix. The coherence length measures the width of the distribution of off-diagonal entries, while the ensemble width measures the spread of the on-diagonal entries. For a free particle, these have identical time dependence. Decoherence causes a reduction in the coherence length over time which is accompanied by an increase in the ensemble width. In reality, the coherence length will only fall to some minimum value related to the energy and length scale of the interaction between the system and environment. However, this minimum is closely related to thermalization and will not appear in simplified models such as the JZME.

Substituting a Gaussian initial state into Eq. (4), we find that the coupling parameter $\gamma(t)$ can be written as

$$\gamma(t) = \frac{2\Lambda}{\hbar}\frac{1}{w(t)}\int_0^t dt' w(t'). \tag{5}$$

Working through the equations of motion, we find that $w(t) = O(t^3)$ and indeed the form of the resulting coupled differential equations for the parameters describing the Gaussians exactly

agree [36]. Setting $w(0) = b$, the characteristic decoherence time is

$$t_b = \frac{\hbar}{\Lambda b^2}, \tag{6}$$

which is the time taken for the coherence length to fall by a factor of $1/e$ (unless otherwise stated, we will be working in units where $b = \hbar = \Lambda = 1$ for the remainder of this paper). The behavior of $\gamma(t)$ can be split into two regimes, short and long times, as

$$\gamma(t) = 2\Lambda t + O(t^2), \quad t \ll t_b \tag{7}$$

$$\gamma(t) = c_0 + \frac{\Lambda t}{2} + O(t^{-1}), \quad t \gg t_b, \tag{8}$$

where c_0 is a constant determined by the initial conditions. The transition between these two regimes occurs around the first decoherence time. In the numerical calculations, we use an interpolation between these two regimes rather than calculating the integral explicitly, even in the Gaussian case. The short-time expansion clearly holds [by Taylor expanding the integral in Eq. (5) around zero, for instance] for an arbitrary time-dependent width (i.e., the second moment) of a general state, where that is well defined. Although the long-time dependence is only exact in the case of Gaussian initial conditions, numerical investigation shows that it shows good agreement with the JZME in general. Furthermore, if we assume that the long-time behavior of the width is dominated by polynomial growth, so that $w(t) = O(t^n)$ for $t \gg t_b$, then it is easily verified that

$$\gamma(t) = \frac{2\Lambda}{\hbar}\frac{\int_0^t dt' w(t')}{w(t)} \propto \frac{t^{n+1}}{t^n} = O(t), \tag{9}$$

which further motivates the general use of a linear time dependence in the limiting (long and short) regimes for a general state.

C. Regularization of the logarithm

Although the limit

$$\lim_{z\to 0} z \log|z| = 0 \tag{10}$$

for $z \in \mathbb{C}$ is straightforward to prove, it is necessary to regularize the logarithm for numerical stability. In particular, we use the regularized logarithmic function $\ln_\sigma$, defined as

$$\ln_\sigma(x) = \mathrm{Re}\ln(x + 10^{-\sigma} i) \tag{11}$$

for some $\sigma \geqslant 0$ so that for $x \gg 0$,

$$\ln_\sigma(x) \approx \ln(x), \tag{12}$$

but as $x \to 0$, $\ln_\sigma(x) \to -\sigma\ln(10)$ rather than diverging to $-\infty$. In the results presented in this paper, $\sigma = 16$, as this was well below the level of desired numerical accuracy and did not noticeably affect the computational resources required. Other choices had little to no appreciable effect on the results, provided $\sigma \gtrsim 2$. Several other regularization schemes were also trialed, including

$$\ln_{(\sigma,N)}(x) = \frac{1}{N}\sum_{k=0}^{N-1} \ln(x + 10^{-\sigma} e^{2\pi i k/N}), \tag{13}$$

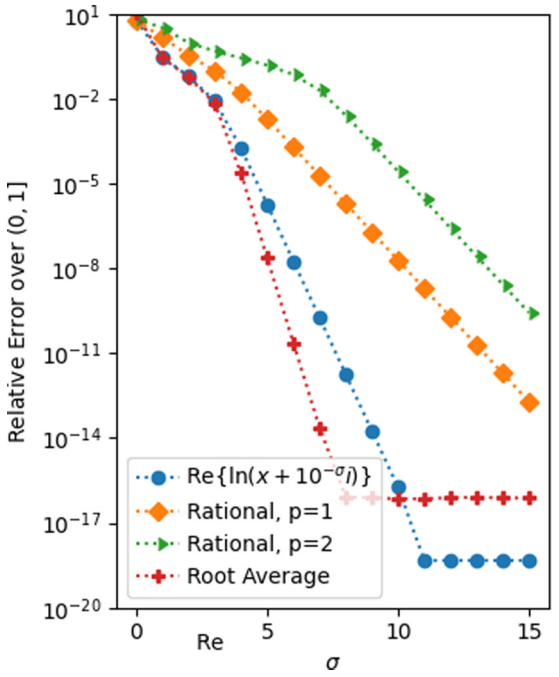

FIG. 1. Relative $L^2(0, 1]$ distance between the natural logarithm and a variety of regularized logarithms as discussed in the text. "Rational" refers to the form given in Eq. (14) and "root average" refers to the form given in Eq. (13).

which also showed no appreciable sensitivity to choices of σ or N provided $\sigma \gtrsim 3$. A slightly different approach took the form

$$\ln r_{(\sigma,r)}(x) = \frac{x^p}{x^p + 10^{-\sigma}} \ln(x + 10^{-\sigma}), \tag{14}$$

which also did not display any appreciable effect on the evolution for $\sigma \gtrsim 3$ and all $p \geqslant 1$. Similar conclusions can be drawn from the graph in Fig. 1, which shows the relative error in terms of the functional distance between the natural logarithm and the various regularization schemes discussed. The functional distance was calculated using the formula

$$\mathrm{Err}(f, g) = \frac{\|f - g\|_2}{\sqrt{\|f\|_2\|g\|_2}} \tag{15}$$

for two functions f and g, where $\|f\|_2$ denotes the $L^2(0, 1]$ norm, given by

$$\|f\|_2 = \left(\int_0^1 dx|f(x)|^2\right)^{1/2}. \tag{16}$$

The fact that the singularity of $z\ln|z|$ at the origin is removable appears to be of much greater importance than the particular method of calculating the logarithm during the intermediate steps. This is consistent with the results of Bao *et al.* [50], which also showed that the evolution to the standard LSE displayed insensitivity to the regularization scheme used.

As discussed in more detail below, particularly in Sec. IV, the behavior of solutions to the LSE near zeros of the wave function disagree significantly with standard theory. However, the results in this section strongly suggest that these issues

appear to be caused not by the numerical details of the logarithmic regularization but by analytic properties of the form of the LSE itself and its derivation from CWT.

We used a split-operator approach with the second-order Strang-splitting scheme to propagate the LSE (see Ref. [50] for a thorough analysis of operator splitting applied to the standard LSE). This has been shown to have better performance in both computational time and reduced numerical error when compared to a (modified) Crank-Nicolson finite-difference scheme which is standard for linear PDEs [51]. Operator splitting also has the advantage of being relatively straightforward to implement, as most of the computation is handled by Fourier transforms. In our case, the algorithm was implemented in PYTHON, using the NUMPY library [52] for array manipulation and Fourier transforms.

D. Error analysis

Although the Strang-splitting method has relatively low numerical error and is stable for the standard LSE [50], CWT requires the nonlinearity to be time dependent. This leads to an intrinsic source of numerical error for any discrete numerical scheme. To see this, consider a general nonlinear Schrödinger-like equation

$$i\partial_t u(x,t) + \tfrac{1}{2}\nabla^2 u(x,t) = F[u(x,t)], \tag{17}$$

where $F[u]$ is some arbitrary differentiable function with the square brackets denoting that F will typically take a function as an argument, although it can also depend on x and t independently. Recall also that in our units $\hbar = m = 1$. We denote some approximate solution to this equation, given by some numerical scheme, for example, by $\tilde{u}$ so that

$$\tilde{u}(x,t) = u(x,t) + \eta(x,t), \tag{18}$$

where $u(x,t)$ is the exact solution and $\eta(x,t)$ is the error. If we try to evolve $\tilde{u}$ using the equation of motion, we find

$$i\partial_t u + \tfrac{1}{2}\nabla^2 u + i\partial_t \eta + \tfrac{1}{2}\nabla^2 \eta = F[u+\eta]. \tag{19}$$

Expanding the right-hand side of this expression as a Taylor series in η,

$$F[u+\eta] = F[u(x,t)] + \sum_{k=1}^{\infty} \frac{\partial^k F[u]}{\partial u^k}\frac{\eta(x,t)^k}{k!}, \tag{20}$$

and substituting this back into the right-hand side of Eq. (19), we can cancel out the exact solution's terms so that we are left with

$$i\partial_t \eta + \frac{1}{2}\nabla^2 \eta = \sum_{k=1}^{\infty} \frac{\partial^k F[u]}{\partial u^k}\frac{\eta(x,t)^k}{k!}, \tag{21}$$

which means that the error of any approximate solution to a nonlinear equation propagates according to a nonlinear equation of its own. For equations with a nonlinearity that is polynomial in the intensity, such as the Gross-Pitaevskii equation (GPE), the right-hand side of (21) will be of finite order. However, in general, the sum will extend over infinitely many terms. Nonetheless, if $\tilde{u}$ is a good approximation, then η can be taken to be small everywhere and we can truncate the series at $k = 1$, that is,

$$\left(i\partial_t + \tfrac{1}{2}\nabla^2\right)\eta(x,t) = F'[u]\eta(x,t) + O(\eta^2), \tag{22}$$

where $F'[u] = \partial F/\partial u$. The differential operator on the left-hand side of (21) shares a Green's function with the homogeneous time-dependent Schrödinger equation over $\mathbb{R}^d$,

$$G(x,t) = i\Theta(t)\left(\frac{i}{2\pi t}\right)^{d/2} e^{-i(x^2/2t)}, \tag{23}$$

where $\Theta(t)$ is the Heaviside step function, such that

$$\left(i\partial_t + \tfrac{1}{2}\nabla^2\right)G(x,t) = \delta^d(x)\delta(t). \tag{24}$$

Although Eq. (22) cannot be solved exactly either, we can extract some information about the behavior of the errors propagated by (21) by expanding the solution in a series $\eta(x,t) = \sum_n \eta_n(x,t)$, where

$$\eta_{n+1} = G * (F'[u]\eta_n), \tag{25}$$

with $*$ denoting convolution. The first term η_0 can be thought of as the error intrinsic to the original approximation and η_n for $n \geqslant 1$ represents error propagated due to the nonlinear nature of the equation of motion. Since the Green's function contains a factor of $t^{-d/2}$, we expect that the higher-order propagated errors will die out quickly. This is indeed the case for the GPE, where $F'[u]$ is not explicitly time dependent. However, in the case of CWT, we have a time-dependent coupling to the nonlinearity and so $F'[u]$ has an approximately linear time dependence. Thus, each iteration of (25) yields a factor of $t^{1-d/2}$. For $d = 1$, this means that the propagated errors will eventually diverge. For $d = 3$, we would expect these errors to die out, whereas for $d = 2$ a more subtle analysis is required. The latter two cases are outside the scope of this paper, though the methods we present can be generalized to higher dimensions and are intended to form the basis of future work.

While we have shown that any numerical scheme for evolving our equation of interest is inherently unstable, we found that the Strang-splitting approach was stable over the timescale required.

III. NUMERICAL RESULTS

A. Gaussian initial conditions

As demonstrated in [36], CWT can exactly reproduce the evolution predicted by the JZME for Gaussian initial conditions. Moreover, CWT allows us to make a so-called linear-time approximation, which simplifies calculations at the cost of accuracy. Even with this simplified approach, we find that some qualitative features are captured by the LSE. Recalling the discussion in Sec. II B, we note that since the coupling to the nonlinearity transitions between two distinct linear regimes, we try an interpolation between them to approximate $\gamma(t)$. That is, our $\gamma(t)$ is given by

$$\gamma(t) = 2\Lambda t[1-\sigma(t)] + \left(c_0 + \frac{\Lambda t}{2}\right)\sigma(t), \tag{26}$$

where $\sigma(t)$ is the function

$$\sigma(t) = \frac{1+\tanh(t-t_b)}{2}. \tag{27}$$

Any sigmoid function can be used for $\sigma(t)$ and the hyperbolic tangent is selected as it offers a good combination of both

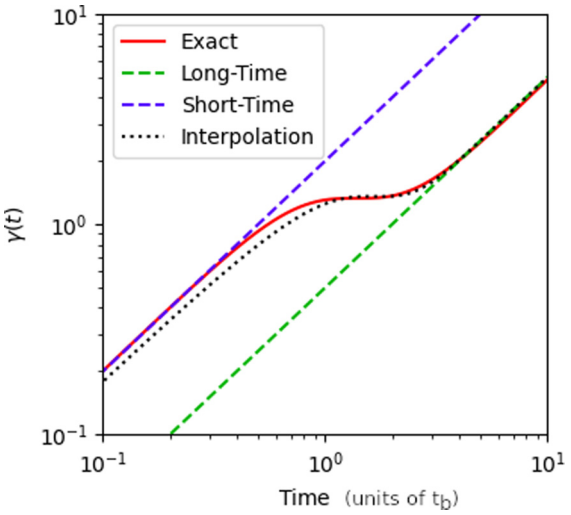

FIG. 2. Behavior of $\gamma(t)$ for a Gaussian state over the timescale of interest, along with its interpolated linear approximation. Note that this is a log-log plot, so straight lines here correspond to straight lines on the equivalent rectangular axes, but offset lines have different gradients, even if they appear parallel.

smoothness of transition and simplicity of implementation. Other widths of the transition (that is, scaling of the time coordinate) can be used, but since we are working in units natural to the problem, the simplest form provides the best agreement.

This linear approximation for $\gamma(t)$ is plotted in Fig. 2. In this manner, we smoothly interpolate between the short- and long-time regimes with a transition over the characteristic decoherence time t_b. Naturally, this does introduce some error, even in the Gaussian case, which can be seen as a slight disagreement between the exact JZME solution and the LSE solution, which is visible in Fig. 3. On the other hand, this approach is reasonably general and simple, as well as being quite flexible, as different interpolation methods could produce better agreement in regions of interest (much shorter than the decoherence timescale or much longer, for example).

Figure 3 was created using a time step of $0.05t_b$ (and in our units $t_b = 1$), a domain of width 30 comprising 2048 points (or a spatial step size of approximately 0.015). The Gaussian initially had a unit standard deviation and a mean of zero.

The apparent interference effects evident after about four decoherence times in Fig. 3 are due to the periodic boundary conditions implicit in the Fourier transforms used to perform the split-operator steps. This leads to one side of the Gaussian wrapping around the domain and interfering with the other half once it has grown sufficiently wide. This can be postponed by simply using a wider domain, although at the expense of a larger number of spatial steps to maintain the same density of points.

B. Non-Gaussian zero-free initial conditions

Two non-Gaussian functions that do not possess zeros were also trialed as initial conditions (see Figs. 4 and 5). These were the Lorentzian, given by

$$a(x,0) = \sqrt{\frac{1/\pi}{b^2 + x^2}} \tag{28}$$

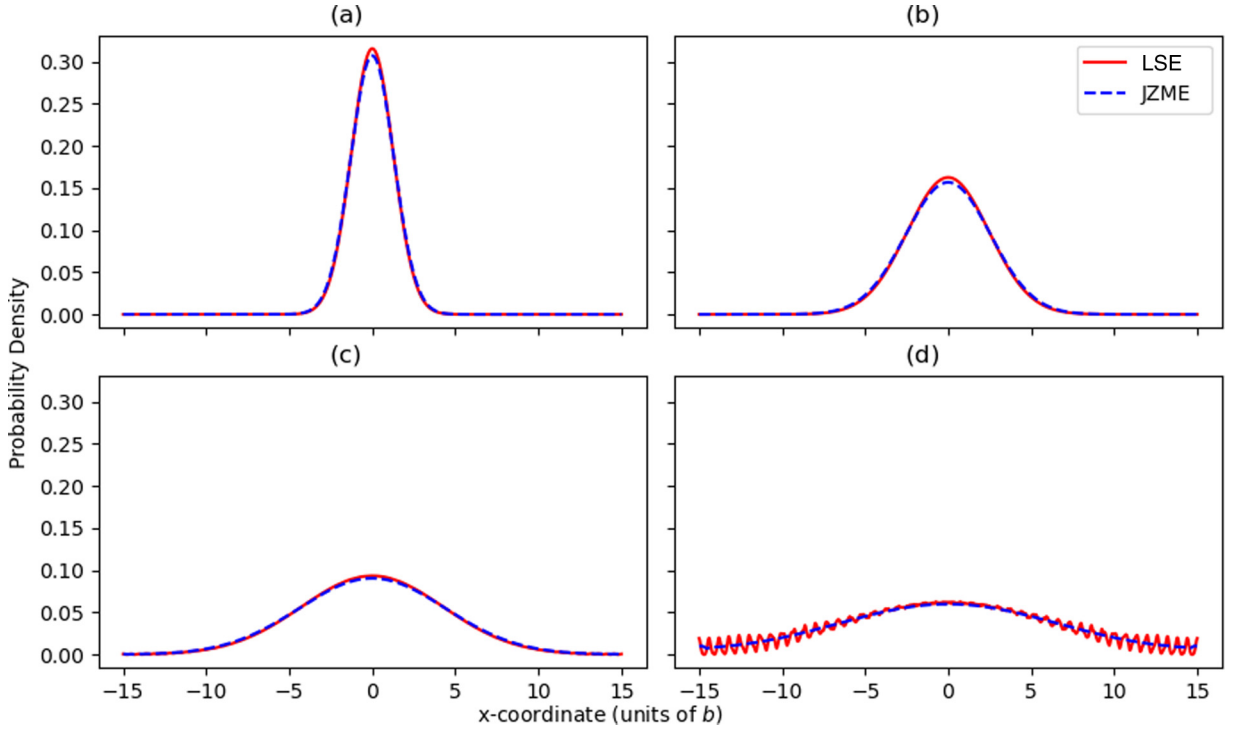

FIG. 3. Gaussian initial conditions propagated by both the JZME and the LSE with the linear-interpolation form $\gamma(t)$ function at multiples of the characteristic decoherence time: (a) $1t_b$, (b) $2t_b$, (c) $3t_b$, and (d) $4t_b$. This demonstrates the good agreement between the two models, until the wave-packet encounters the boundary. The origin of the interference fringes is discussed in the text.

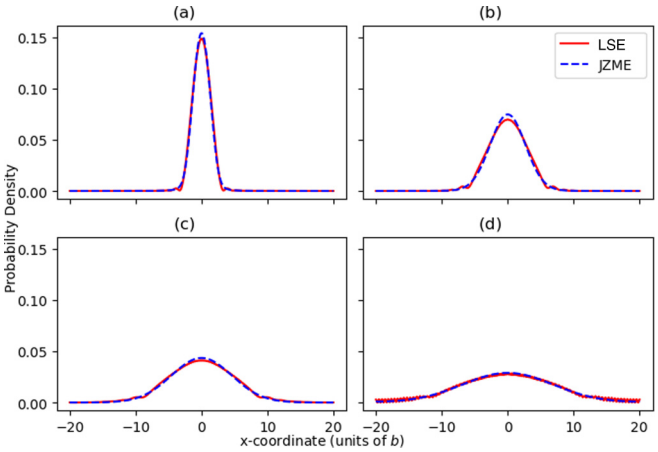

FIG. 4. An initially Lorentzian wave function evolving under both the JZME and LSE with the linearly interpolated form of $\gamma(t)$ at multiples of the decoherence time: (a) $1t_b$, (b) $2t_b$, (c) $3t_b$, and (d) $4t_b$. Although zero-pinning effects, discussed in detail in Sec. IV, are visible, the ensemble width shows good agreement between the two methods.

for a width parameter b, and the hyperbolic secant, given by

$$a(x,0) = \frac{1}{\sqrt{2b}}\mathrm{sech}\left(\frac{x}{b}\right) = \sqrt{\frac{2}{b}}\left[\exp\left(\frac{x}{b}\right) + \exp\left(-\frac{x}{b}\right)\right]^{-1} \tag{29}$$

with an analogous width parameter b. Note that the width parameter for the Lorentzian represents half the full width at half maximum and not the standard deviation, since the latter is ill-defined for a Lorentzian distribution.

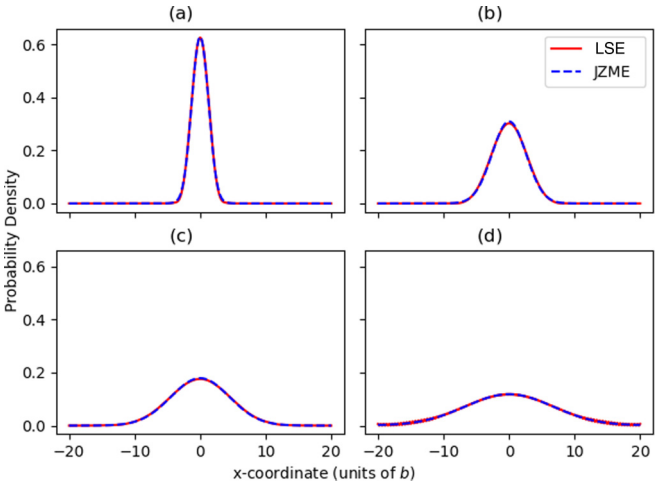

FIG. 5. Wave function initially described by the hyperbolic secant evolving under both the JZME and LSE with the linearly interpolated form of $\gamma(t)$ at multiples of the decoherence time: (a) $1t_b$, (b) $2t_b$, (c) $3t_b$, and (d) $4t_b$. Since zeros do not develop during evolution, the agreement between the two methods is very good until finite domain effects cause spurious interference effects, similar to the Gaussian case. The origin of these effects is discussed in the text.

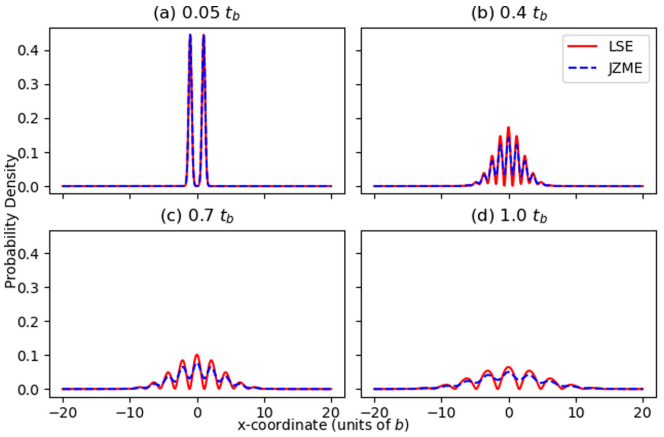

FIG. 6. Twin Gaussian initial conditions at various fractions of the characteristic decoherence time: (a) $0.05t_b$, (b) $0.4t_b$, (c) $0.7t_b$, and (d) $1.0t_b$. As in Fig. 3, the LSE is implemented with the linearly interpolated form of $\gamma(t)$. This demonstrates the good agreement in the ensemble width behavior of the LSE solution, while the zero-pinning effects, discussed further in Sec. IV, are evident.

C. Double-peak initial conditions

For non-Gaussian initial conditions, we observe a phenomenon we have termed zero pinning whereby the number of points of zero intensity in the wave function do not decrease as a result of the evolution under the LSE. This is particularly evident in Fig. 6, where the initial marginal wave function is a coherent superposition of two Gaussians, of the form

$$a(x,0) = N(b,s)^{-1/2}\left[\exp\left(-\frac{(x-s)^2}{4b^2}\right) + \exp\left(-\frac{(x+s)^2}{4b^2}\right)\right], \tag{30}$$

where $N(b,s)$ is a normalization factor. We choose $s = b = 1$ in our units, so the peaks are initially of unit width and separated by two units. Again, we used a time step of 0.05 and a spatial step size of approximately 0.015 (a 30-unit-wide domain with 2048 points).

As the two Gaussian peaks spread out, they begin to interfere, creating zeros in the probability distribution. The zeros spread out at the correct rate, but their visibility is not diminished, unlike solutions to the JZME. This represents a significant drawback to using the LSE as a model of decoherence, as decreased fringe visibility is a central feature of decoherence, and is used extensively in experimental work to characterize the decohering effect of the environment [9]. The analytic nature of this problem is discussed further in Sec. IV.

In all test cases where zeros were present, zero pinning was observed. There is no sensitivity to the origin of the zero, whether it is a feature of the initial conditions or interference effects (such as the twin-Gaussian case shown above) or as a result of dynamics (for example, an isolated Cauchy-Lorentz distribution will spontaneously form zeros as it spreads out). As discussed below, this is likely a result of the analytic properties of the LSE and not a numerical artifact. Moreover, even with the zero pinning, all test cases showed good

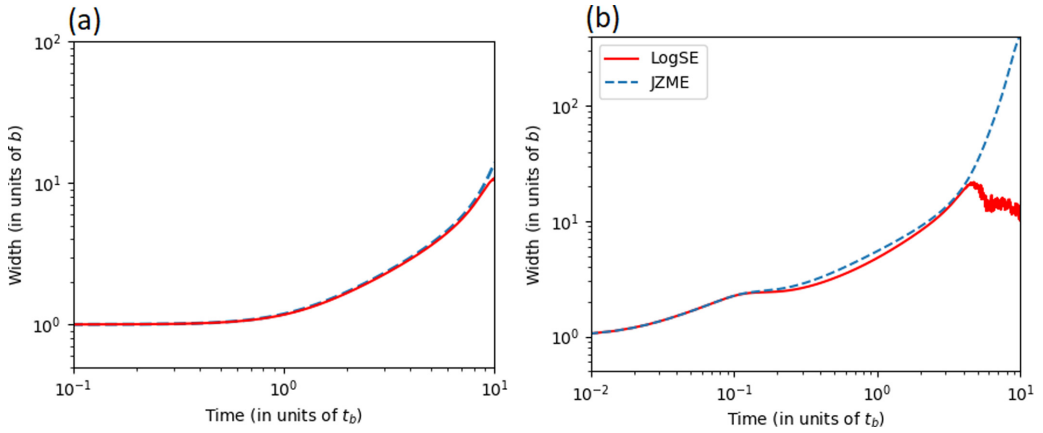

FIG. 7. Plots of the ensemble widths of the probability distributions corresponding to (a) the Gaussian initial state and (b) the twin-Gaussian initial state, measured relative to the initial width of the distribution [$w(0) = b$]. Note that the kink that occurs in the twin-Gaussian plot at around $10^{-1}t_b$ corresponds to the initial formation of the interference fringes. The divergence of the widths just before $10t_b$ corresponds to the numerical breakdown discussed in Sec. II D.

agreement with the predictions of the JZME regarding the time dependence of the ensemble widths of the distributions.

Note that since the same numerical integrator was used for both the JZME and LSE, the JZME solutions simulated here also have implicitly periodic boundary conditions. Their interference effects are not visible here, however, since the JZME does not exhibit zero pinning and appears to be somewhat more efficient at suppressing the off-diagonal terms in the density matrix.

Conversely, the use of the same integrator for both formalisms resulted in a good demonstration of the significant computational speedup offered by the LSE model. Performing the calculations (on a commercial PC CPU) to produce the figures in this paper took on the order of hours for the highest spatial resolution calculations using the JZME but took only a few minutes using the LSE.

However, operator splitting is not necessarily the most efficient method for propagating the JZME, as it is linear in the density matrix. Generally, finite-difference methods (such as the well-established implicit Crank-Nicolson method) may exhibit better performance for these types of partial differential equations. Nonetheless, the observed reduction in computation time still serves as a comparison to demonstrate a potential advantage of the LSE model.

D. Widths and error growth

Although solutions to the LSE display different behavior from the corresponding JZME solutions, there is good agreement in the behavior of the ensemble-width spreading, as shown in Fig. 7. Note that the kink present around $0.1t_b$ in Fig. 7(b) corresponds to the initial moment the interference fringes form, which affects the growth rate of the width. This is because the fringes contain less probability mass far away from the origin and instead concentrate it in the central band.

As discussed in Sec. II D, the growth in numerical error for a one-dimensional simulation of the LSE grows over time regardless of numerical details. At the same time this error is being propagated, the typical (absolute) value of the wave function is shrinking due to the rapid ensemble width growth (rapid, that is, compared to the free Schrödinger equation solution with the same initial conditions). Since the logarithm rapidly approaches an asymptote for real arguments in (0,1], the function is quite steep in this region. Consequently, small changes in the absolute value of the wave function can have a considerable effect on the value of the logarithm, which may contribute to numerical instability.

The self-interference caused by the periodic boundary conditions can occur quite early in the simulation due to the rapid spreading out of the wave function. Combined with the zero pinning, these effects can be difficult to tease apart by varying the parameters of the simulation (temporal and spatial resolutions, domain size, etc.).

Incorporation of absorptive boundary conditions was attempted in order to mitigate the effects of self-interference, but were ultimately disregarded. An imaginary potential that was nonzero only at the boundary was trialed; however, unless the width of this nonzero region was carefully tuned, reflections from the boundary were produced ([53] contains a good discussion of this problem). This tuning seemed to be sensitive to the initial conditions, unlike in the linear case, and simply introduced a new problem while not completely eliminating the wrapping of the wave function around the domain. While more mathematically rigorous and physically realistic methods exist for implementing absorptive boundary conditions, these can introduce significant computational complexity because they require an additional integral to be performed at each time step, as well as being nonlocal in time (see [54] for an example algorithm and general analysis).

Ultimately, the computational scaling of integrating the LSE with Strang-splitting means that it is in general more tractable to simply work with a very large domain to mitigate the spurious effects of periodicity.

Regardless, the good agreement between the two formalisms (master equation versus LSE) as far as the ensemble width is concerned suggests that while the form of the LSE that has been derived captures some aspects of the environmental influence, the mechanism by which fringe visibility is diminished is lost. Interestingly this also suggests that these are, in some sense, separate phenomena, which is not obvious

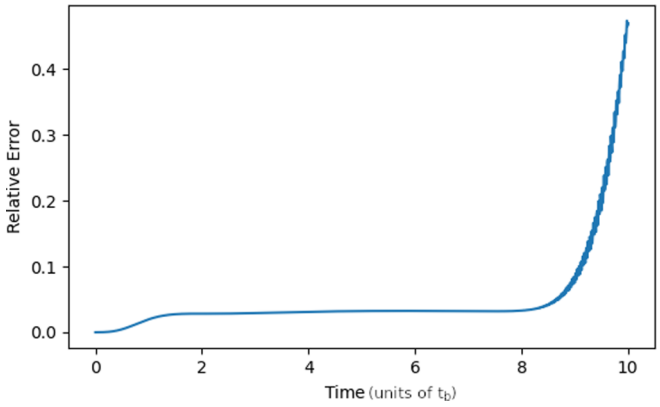

FIG. 8. Relative L^2 error (defined in the text) of the JZME and LSE evolutions of a Gaussian initial state. The rapid increase in error around nine characteristic times is insensitive to the domain width and spatial resolution, corresponding to the inevitable numerical breakdown discussed in Sec. II D.

a priori, since both appear simultaneously with the addition of the single decohering term in the JZME.

IV. DISCUSSION

As shown in Fig. 8, the LSE performs very well as a model of decoherence for a Gaussian initial state. In all other test cases investigated, the LSE yielded ensemble width growth that closely matched the JZME solution, before numerical instability set in. Since the LSE's computational demand scales more favorably than the master-equation approach, it is not unreasonable to decrease the step size somewhat in order to improve stability. However, as shown in Fig. 9, this only delays the breakdown to a point. As discussed in Sec. II D, the time dependence of the nonlinearity all but guarantees a finite-time numerical breakdown.

Furthermore, our analysis indicates that in more than one dimension, the accumulation of error intrinsic to the nonlinearity of the problem should not prove as destructive. As discussed above, this is a consequence of the form of the Green's function in Eq. (23). This is of particular interest as the computational speedup offered by conditional wave theory is also most evident in higher-dimensional problems. This suggests that the application of conditional wave theory to quantum-mechanical problems involving continuous degrees of freedom, such as matter-wave interferometry or decoherence of quantum states of matter, could be a promising area for further research. Besides ensemble width growth, the other major prediction of decoherence theory is the loss of fringe visibility in interference patterns. As discussed in Sec. III, the LSE in this form cannot reproduce this behavior. This is a significant hurdle in the way of using this model in practical situations such as prediction of matter-wave interference patterns. The cause of this problem is discussed in the next section, and possible areas of investigation which may offer a solution are proposed.

Zero pinning

We now discuss in depth the mathematical origin of the zero-pinning phenomenon, as this is the most significant drawback of the LSE model. Furthermore, the way that the LSE treats zeros so differently from other values of the wave function suggests that some important mathematical structure is missing or incorrect in the derivation of the LSE from CWT. Although several approximations have been made, it is not immediately apparent how these would result in the observed effects. For example, most of the approximations make no reference to the on-diagonal values of the density matrix or are concerned with simplifying the time dependence of the nonlinear coupling. Although the zero pinning is time independent (in that it occurs regardless of how far along in time the simulation is) we will show that the assumption that the evolution is dependent on purely local information contained in the wave function is closely related to the appearance of zero-pinning effects.

Assume that at some point on the z axis, say, $2x_0$, the intensity $\rho(x_0, x_0)$ goes to zero. We now consider why the addition of a term proportional to $y^2\rho(y, z)$ in the master equation should fill in the zero when this term vanishes at this point. To begin, we note that along the z axis ρ must be real

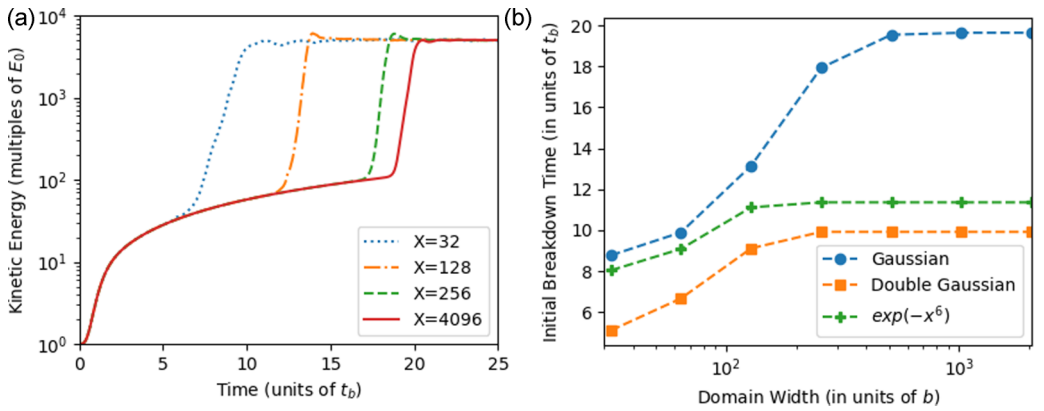

FIG. 9. (a) Kinetic energy of a Gaussian state plotted against time, in units of the initial kinetic energy. Initially, the kinetic energy grows linearly (note the logarithmic axis) and suddenly jumps when the wave packet encounters the edge and wraps around the domain. (b) Point at which this jump first occurs, plotted with increasing domain width. Note that for domains wider than about $10^3 b$, the numerical breakdown is no longer due to self-interference, but is intrinsic to the LSE as we have implemented it.

and a short distance along this axis, say, δx, from the point x_0, ρ must be small, positive, and approximately parabolic. This follows if the zero is of first order in the wave function. If we Taylor expand in time around the zero (assuming ρ vanishes at some time t), we find

$$\rho(x_0, x_0, t + dt) = dt\left(\frac{i}{\mu}\partial_{yz}^2\rho - \lambda y^2\rho\right) + \frac{dt^2}{2}\left(\frac{i}{\mu}\partial_{yz}^2\dot{\rho} - \lambda y^2\dot{\rho}\right) + \frac{dt^3}{3!}\left(\frac{i}{\mu}\partial_{yz}^2\ddot{\rho} - \lambda y^2\ddot{\rho}\right) + O(dt^4), \tag{31}$$

where $\mu^{-1} = 2\hbar/m$, $\lambda = \Lambda/\hbar$, the overdots denote differentiation with respect to time, and everything on the right-hand side is understood as being evaluated at the point (x_0, x_0) at time t. We can find the expressions for the higher time derivatives of ρ by repeated application of the JZME (A2). A significant amount of algebraic work can be saved by noting that most of the terms generated in this manner will vanish. Trivially, anything with a surviving factor of y must be zero, since this clearly vanishes at (x_0, x_0). Furthermore, the derivative operator can be rewritten

$$\partial_{yz}^2\rho = \tfrac{1}{4}\left(\partial_x^2\rho - \partial_{x'}^2\rho\right), \tag{32}$$

but since ρ vanishes along both of the axes (s, x_0) and (x_0, s) (where $s \in \mathbb{R}$) the second derivatives with respect to both x and x' must both vanish at (x_0, x_0). From all this, we can conclude that both the first- and second-order-in-time terms vanish, but the third-order term will contain

$$\dddot{\rho} \sim \left(\frac{i}{\mu}\frac{\partial^2}{\partial y \partial z}\right)^2(-\lambda y^2\rho) \sim \frac{2\lambda}{\mu^2}\frac{\partial^2\rho}{\partial z^2} \approx \frac{16\hbar\Lambda}{m}\frac{\rho_\delta}{\delta x^2}, \tag{33}$$

where $\sim$ denotes equality up to cancellation of terms that vanish according to our observations above and ρ_δ is the value of $\rho(x, x)$ a short distance in either direction along the z axis. As we noted, ρ is approximately parabolic along this axis and so the second derivative along it is positive (since ρ must be non-negative along z). Thus, for short times, the growth of absolute value of the wave function will be cubic in time.

Note this argument depends crucially on the fact that the JZME is manifestly nonlocal. Information about the state at the point x' is propagated to x through the decoherence term encountering the kinetic term. In the LSE all information remains local and so cannot be propagated to fill in the zeros.

A similar analysis can be performed for the LSE. To begin, the marginal wave function can be expanded over some small time step dt at some first-order zero x_0 and eliminating terms that vanish at the zero,

$$a(x_0, t + dt) = dt^2\frac{1}{m}\nabla\varepsilon\cdot\nabla a + O(dt^3), \tag{34}$$

recalling that $\nabla^2 a = 0$ at a first-order zero. Furthermore, from the derivation of the LSE (detailed in the Appendix) the gradient of $\varepsilon(x)$ is given by

$$\frac{\partial\varepsilon(x)}{\partial x} = -\frac{\hbar^2}{m}\frac{1}{|a(x)|}\frac{\partial}{\partial x}\{|a(x)|\gamma(x)\} \tag{35}$$

so that

$$a(x_0, t + dt) = -\frac{dt^2}{2}\frac{\hbar^2}{m^2}\frac{1}{|a|}\frac{\partial}{\partial x}\{|a(x)|\gamma(x)\}\frac{\partial a}{\partial x}. \tag{36}$$

Setting $\hbar = m = 1$, the coefficient of dt^2, c_2, can be written

$$c_2 = \frac{\partial\gamma}{\partial x}\frac{\partial a}{\partial x} + \frac{\gamma}{|a|}\frac{\partial|a|}{\partial x}\frac{\partial a}{\partial x}, \tag{37}$$

which appears to be singular at the zero, since $|a| \to 0$. However, care must be taken, since that is also precisely the point at which $|a|$ is not differentiable. Expanding over some small step dx using a central finite difference and setting $|a(x)| = r(x)$,

$$\lim_{x\to x_0}\frac{1}{|a(x)|}\frac{\partial|a(x)|}{\partial x} \tag{38}$$

$$= \lim_{x\to x_0}\frac{1}{r(x)}\lim_{dx\to 0}\frac{r(x + dx/2) - r(x - dx/2)}{dx} \tag{39}$$

$$= \lim_{x\to x_0}\frac{r'(x_0^+) + r'(x_0^-)}{r(x)}. \tag{40}$$

Note that close to a zero, $f'(x_0^+) = -f'(x_0^-)$ for any continuous real function f. So it must hold that

$$\lim_{x\to x_0}\frac{1}{|a(x)|}\frac{\partial|a(x)|}{\partial x} = \lim_{x\to x_0}\frac{0}{r(x)} = 0. \tag{41}$$

The second term of c_2 in Eq. (37) can therefore be dropped, leaving

$$a(x_0, t + dt) = -dt^2\frac{\hbar^2}{m^2}\gamma'(x_0, t)a'(x_0, t), \tag{42}$$

which is clearly nonzero if a is not everywhere zero and γ is a function of space. In the simplest version of the CWT LSE that we have used so far, γ is not a function of space, implying that $\gamma'(x) = 0$, which in turn means the zeros cannot be filled in.

Following the derivation of the LSE given in the Appendix, we can arrive at a slightly more general solution for the nonlinear term than is given in Eq. (4),

$$\varepsilon(x, t) = C(t) - \int_0^x dx'\frac{1}{|a(x', t)|}\frac{\partial[\gamma(x', t)|a(x', t)|]}{\partial x'}, \tag{43}$$

where $C(t)$ is an arbitrary function of time that does not affect the dynamics. If we allow γ to be independent of x' then we recover our expression for the logarithmic nonlinearity. In general, however, ε can be written

$$\varepsilon(x, t) = -\gamma(x, t) - \int_0^x dx'\gamma(x', t)\frac{\partial}{\partial x'}\ln|a(x', t)|, \tag{44}$$

which follows from the product rule applied to the integrand of Eq. (43), and the constant of integration has been set to zero. This form suggests that the influence of the coupling to the environment manifests in two ways. The first term represents a local potential which arises directly from the interaction with the environment and a second, nonlocal term is difficult to interpret physically. Zloshchastiev [55] discussed the logarithmic Schrödinger equation in the context of quantum information transfer, and the above form of the nonlinear term suggests a kind of weighted sum over the differential information content of the probability distribution generated

by the marginal wave function. Thus the integral term may be interpreted as the amount of entanglement with the environment, as measured by the delocalized quantum information content of the marginal state. The principal challenge in applying Eq. (44) unsurprisingly lies in evaluating the integral. First, at points where the magnitude of the wave function vanishes, the logarithm is ill-defined. However, this does not mean that the integral itself is undefined. If we regard x as the real part of a complex coordinate, it is possible to evaluate the integral assuming the marginal magnitude is meromorphic on an appropriate domain. This can be done using the generalized Cauchy argument principle, which states that for a meromorphic function f and a holomorphic function g of a complex variable w, defined on an open subset of the complex plane D,

$$\frac{1}{2\pi i}\oint_C dw\frac{f'(w)}{f(w)}g(w)=\sum_z g(z)n_C(z)-\sum_p g(p)n_C(p), \tag{45}$$

where C is a closed curve in D that does not intersect the zeros (z) or poles (p) of f and $n_C(x)$ is the winding number of the point x with respect to the curve C [note that if x does not lie in the interior of C, $n_C(x)=0$]. Currently, we know of no sufficiently general solution for $\gamma(x,t)$ to actually apply this formula or how to find such a solution numerically. Nonetheless, the importance of zeros in the generalized Cauchy argument principle, along with the seemingly reasonable assumption that there should not be any poles in $|a(x,t)|$ on the real line, is suggestive of a possible resolution to the zero-pinning problem.

V. CONCLUSION

Conditional wave theory offers new mathematical tools for the analysis of quantum decoherence, a central problem in the era of emerging quantum technologies. We have shown that as applied to the localizing effects of decoherence, as measured by the behavior of the ensemble width of a state, the logarithmic equation of motion predicted by CWT demonstrates excellent agreement with standard theory. However, the mathematically simplest form of this equation of motion leads to significant accumulation of error and zero-pinning behavior. We have shown that the former is accompanied by intrinsic reduction of necessary computational resources, by working at the wave-function level, and becomes less problematic with increasing dimension. The zero-pinning effect prevents the destruction of interference effects that are well known to occur as a result of decoherence. The resolution of this shortcoming of CWT may lie in careful analysis of the subtle nonlocal behavior of the coupling to the environment, which appears to have mathematical links to previous work on information theory and the logarithmic Schrödinger equation.

APPENDIX: DERIVATION OF THE LSE

The one-dimensional JZME for the reduced density matrix $\rho_S(x,x')$ can be written in the standard form

$$\frac{d\rho_S(x,x',t)}{dt}=\frac{i\hbar}{2m}\left(\frac{\partial^2}{\partial x^2}-\frac{\partial^2}{\partial x'^2}\right)\rho_S(x,x')-\frac{\Lambda}{\hbar}(x-x')^2\rho_S(x,x'). \tag{A1}$$

It is more convenient to work in the rotated coordinate system given by $y=x-x'$ and $z=x+x'$. The JZME thus becomes

$$\frac{d\rho_S(y,z,t)}{dt}=\frac{2i\hbar}{m}\frac{\partial^2}{\partial y\partial z}\rho_S(y,z,t)-\frac{\Lambda}{\hbar}y^2\rho_S(y,z,t). \tag{A2}$$

The evolution of solutions to the JZME is characterized by the narrowing of the distribution of nonzero density-matrix entries around $y=0$, i.e., the diagonal. The key insight of CWT is that this single master equation can be written as two equations for the conditional and marginal wave functions $\phi(x,q,t)$ and $a(x,t)$, respectively, where the total system-environment wave function $\psi(x,q,t)$ is given by

$$\psi(x,q,t)=\phi(x,q,t)a(x,t), \tag{A3}$$

where the generalized coordinate q represents the degree(s) of freedom of the environment. The reduced density matrix is then given by

$$\rho_S(x,x',t)=\mathrm{tr}_E\psi^*(x',q',t)\psi(x,q,t)=\int dq\,\psi^*(x',q,t)\psi(x,q,t). \tag{A4}$$

Substituting in the CWT factorization, we find

$$\rho_S(x,x',t)=a^*(x',t)a(x,t)\int dq\,\phi^*(x',q,t)\phi(x,q,t)=\rho_M(x,x',t)K(x,x',t), \tag{A5}$$

where we defined the marginal density matrix $\rho_M(x,x',t)=a^*(x',t)a(x,t)$ and the coherence integral $K(x,x',t)=\int dq\,\phi^*(x',q,t)\phi(x,q,t)$. Substituting this back into the JZME (A2), we find that the marginal density matrix and the coherence integral must satisfy

$$\frac{d\rho_M}{dt}=\frac{2i\hbar}{m}\left(\partial_{yz}\rho_M+(\partial_y\rho_M)(\partial_z\ln K)+(\partial_z\rho_M)(\partial_y\ln K)+\rho_M\frac{\partial^2_{yz}K}{K}\right)-\frac{\Lambda}{\hbar}y^2\rho_M-\frac{d}{dt}\ln K. \tag{A6}$$

However, CWT also requires that the marginal density matrix obey an equation of motion of its own [36]. This arises from the equation of motion for the marginal wave function, which itself arises from the Schrödinger equation, the CWT factorization, Eq. (A3), and the requirement

$$\int dq\,\phi^*(x,q,t)\phi(x,q,t)=1. \tag{A7}$$

With an appropriate choice of gauge, the equation of motion for the marginal wave function can be written as

$$i\frac{da(x,t)}{dt}=-\frac{\hbar}{2m}\frac{\partial^2 a(x,t)}{\partial x^2}+\frac{1}{\hbar}\varepsilon(x,t)a(x,t), \tag{A8}$$

where $\varepsilon(x,t)$ is a real-valued function. This leads to an equation of motion for the marginal density matrix through the relation $\rho_M(x,x',t)=a^*(x',t)a(x,t)$,

$$\frac{d\rho_M}{dt}=\frac{i\hbar}{2m}\left(\partial_x^2-\partial_{x'}^2\right)\rho_M-\frac{i}{\hbar}[\varepsilon(x,t)-\varepsilon(x',t)]\rho_M. \tag{A9}$$

Our aim then is to find a form of $\varepsilon(x,t)$ and $K(x,x',t)$ such that Eqs. (A9) and (A6) are equivalent. One such form can be found by noting the fact that the original JZME has analytic

Gaussian solutions, suggesting that a Gaussian form for K may satisfy this requirement. In particular, if we take

$$K(y,t) = \exp\left(-\frac{\gamma(t)y^2}{2}\right), \tag{A10}$$

where we are working in the (y,z) basis for convenience, then it can be verified by substitution that Eqs. (A6) and (A9) coincide as $y \to 0$ provided

$$\varepsilon(x,t) = \frac{\hbar^2}{m}\gamma(t)\ln|a(x,t)|^2. \tag{A11}$$

For $y \neq 0$, the two equations coincide only if

$$\frac{d\gamma(t)}{dt} = \frac{\Lambda}{\hbar} \Rightarrow \gamma(t) = \gamma(0) + \frac{\Lambda t}{\hbar}. \tag{A12}$$

However, since all observables depend only on the diagonal values of $\rho_M(x,x')$, that is, when $x = x'$ or equivalently $y = 0$, the requirement of the evolution of the off-diagonal terms is not strictly necessary. In the Gaussian case, for example, Eq. (A12) does not hold for all time, but still shows good agreement with the JZME, as discussed in the main text. A more general solution can be found by dropping the Gaussian assumption for $K(x,x',t)$. The expression for $\varepsilon(x,t)$ in that case has the form

$$\varepsilon(x,t) = C(t) + \int_0^x dx'\gamma_2(x',t)\frac{\partial}{\partial x'}\ln[\gamma_2(x',t)r(x',t)], \tag{A13}$$

where $r(x,t) = |a(x,t)|$, $C(t)$ is an arbitrary function of time which does not affect the dynamics, and $\gamma_2(x,t)$ is defined as

$$\gamma_2(x,t) = \frac{\partial^2}{\partial y^2}\ln K(y,z,t)\bigg|_{y=0}. \tag{A14}$$

Equation (A13) can be verified by substitution of

$$\frac{\gamma(t)y^2}{2} \to \sum_n \frac{\gamma_n(z,t)y^n}{n!} \tag{A15}$$

in Eq. (A10). This agrees with the Gaussian case exactly when $\frac{\partial\gamma_2}{\partial x} = 0$, which is to say that $\gamma_n = 0$ for $n > 2$.

[1] M. Schlosshauer, Rev. Mod. Phys. **76**, 1267 (2005).
[2] M. Schlosshauer, *Decoherence and the Quantum-to-Classical Transition* (Springer, Berlin, 2007).
[3] E. Joos and H. D. Zeh, Z. Phys. B **59**, 223 (1985).
[4] L. Duan, M. D. Lukin, J. I. Cirac, and P. Zoller, Nature (London) **414**, 413 (2001).
[5] A. M. Tyryshkin, S. Tojo, J. J. L. Morton, H. Riemann, N. V. Abrosimov, P. Becker, H.-J. Pohl, T. Schenkel, M. L. W. Thewalt, K. M. Itoh, and S. A. Lyon, Nat. Mater. **11**, 143 (2012).
[6] G. Lindblad, Commun. Math. Phys. **48**, 119 (1976).
[7] M. R. Gallis and G. N. Fleming, Phys. Rev. A **42**, 38 (1990).
[8] K. Hornberger and J. E. Sipe, Phys. Rev. A **68**, 012105 (2003).
[9] M. Arndt, Phys. World **18**, 35 (2005).
[10] W. H. Zurek, Rev. Mod. Phys. **75**, 715 (2003).
[11] Y. Colombe, T. Steinmetz, G. Dubois, F. Linke, D. Hunger, and J. Reichel, Nature (London) **450**, 272 (2007).
[12] A. O. Caldeira and A. J. Leggett, Physica A **121**, 587 (1983).
[13] R. P. Feynman and F. L. Vernon, Jr., Ann. Phys. (NY) **24**, 118 (1963).
[14] C. H. Fleming, A. Roura, and B. L. Hu, Ann. Phys. (NY) **326**, 1207 (2011).
[15] Y. Makhlin, G. Schön, and A. Shnirman, Rev. Mod. Phys. **73**, 357 (2001).
[16] T. Pellizzari, S. A. Gardiner, J. I. Cirac, and P. Zoller, Phys. Rev. Lett. **75**, 3788 (1995).
[17] J. L. O'Brien, A. Furusawa, and J. Vučković, Nat. Photon. **3**, 687 (2009).
[18] L. Tian, S. Lloyd, and T. P. Orlando, Phys. Rev. B **65**, 144516 (2002).
[19] H. J. Groenewold, Physica **12**, 405 (1946).
[20] J. E. Moyal, Math. Proc. Camb. Philos. Soc. **45**, 99 (1949).
[21] E. P. Wigner, Phys. Rev. **40**, 749 (1932).
[22] T. Curtright and C. Zachos, Asia Pac. Phys. Newsl. **01**, 37 (2012).
[23] J. Bateman, S. Nimmrichter, K. Hornberger, and H. Ulbricht, Nat. Commun. **5**, 4788 (2014).
[24] C. C. López and J. P. Paz, Phys. Rev. A **68**, 052305 (2003).
[25] P. Milman, A. Auffeves, F. Yamaguchi, M. Brune, J. Raimond, and S. Haroche, Eur. Phys. J. D **32**, 233 (2005).
[26] A. L. Matacz, Phys. Rev. D **49**, 788 (1994).
[27] N. Gisin and I. C. Percival, J. Phys. A: Math. Gen. **25**, 5677 (1992).
[28] N. Gisin and I. C. Percival, J. Phys. A: Math. Gen. **26**, 2245 (1993).
[29] G. C. Ghirardi, A. Rimini, and T. Weber, Phys. Rev. D **34**, 470 (1986).
[30] G. C. Ghirardi, P. Pearle, and A. Rimini, Phys. Rev. A **42**, 78 (1990).
[31] L. Diósi, Phys. Lett. A **120**, 377 (1987).
[32] R. Penrose, Gen. Relat. Gravit. **28**, 581 (1996).
[33] E. Platen, Acta Numer. **8**, 197 (1999).
[34] A. Shapiro, Handb. Oper. Res. Manage. Sci. **10**, 353 (2003).
[35] D. Kroese, T. Taimre, and Z. Botec, *Handbook of Monte Carlo Methods* (Wiley Blackwell, Hoboken, 2011).
[36] R. van Geleuken and A. V. Martin, Phys. Rev. Research **2**, 033189 (2020).
[37] G. Hunter, Int. J. Quantum Chem. **9**, 237 (1975).
[38] A. Abedi, N. T. Maitra, and E. K. U. Gross, Phys. Rev. Lett. **105**, 123002 (2010).
[39] N. M. Hoffmann, H. Appel, A. Rubio, and N. T. Maitra, Eur. Phys. J. B **91**, 180 (2018).
[40] S. K. Min, F. Agostini, and E. K. U. Gross, Phys. Rev. Lett. **115**, 073001 (2015).
[41] B. F. E. Curchod, F. Agostini, and E. K. U. Gross, J. Chem. Phys. **145**, 034103 (2016).
[42] B. D. Forbes, A. V. Martin, S. D. Findlay, A. J. D'Alfonso, and L. J. Allen, Phys. Rev. B **82**, 104103 (2010).
[43] I. Bialynicki-Birula and J. Mycielsky, Ann. Phys. (NY) **100**, 62 (1976).
[44] I. Bialynicki-Birula and J. Mycielski, Phys. Scr. **20**, 539 (1979).
[45] C. G. Shull, D. K. Atwood, J. Arthur, and M. A. Horne, Phys. Rev. Lett. **44**, 765 (1980).

[46] E. F. Hefter, Phys. Rev. A **32**, 1201 (1985).
[47] M. Shen, Q. Wang, J. Shi, Y. Chen, and X. Wang, Phys. Rev. E **72**, 026604 (2005).
[48] K. G. Zloshchastiev, Acta Phys. Pol. B **42**, 261 (2011).
[49] A. Avdeenkov and K. G. Zloshchastiev, J. Phys. B **44**, 195303 (2011).
[50] W. Bao, R. Carles, C. Su, and Q. Tang, Numer. Math. **143**, 461 (2019).
[51] W. Bao, R. Carles, C. Su, and Q. Tang, SIAM J. Numer. Anal. **57**, 657 (2019).
[52] C. R. Harris, K. J. Millman, S. J. van der Walt, R. Gommers, P. Virtanen, D. Cournapeau, E. Wieser, J. Taylor, S. Berg, N. J. Smith, R. Kern, M. Picus, S. Hoyer, M. H. van Kerkwijk, M. Brett, A. Haldane, J. F. del Río, M. Wiebe, P. Peterson, P. Gérard-Marchant *et al.*, Nature (London) **585**, 357 (2020).
[53] F. He, C. Ruiz, and A. Becker, Phys. Rev. A **75**, 053407 (2007).
[54] C. Lubich and A. Schädle, SIAM J. Sci. Comput. **24**, 161 (2002).
[55] K. G. Zloshchastiev, Z. Naturforsch. A **73**, 619 (2018).